Thin Solid Films 691 (2019) 137587

Contents lists available at ScienceDirect

Thin Solid Films

journal homepage: www.elsevier.com/locate/tsf

High performance piezoresistive response of nanostructured ZnO/Ag thin films for pressure sensing applications

Armando Ferreira[a,*], João Paulo Silva[a], Rui Rodrigues[a], Nicolas Martin[b], Senentxu Lanceros-Méndez[c,d], Filipe Vaz[a]

[a] Centro de Física, Universidade do Minho, 4710-057 Braga, Portugal
[b] Institut FEMTO-ST, UMR 6174 CNRS, Univ. Bourgogne Franche-Comté, 15B Avenue des Montboucons, 25030 Besançon Cedex, France
[c] BCMaterials, Basque Center for Materials, Applications and Nanostructures, UPV/EHU Science Park, 48940 Leioa, Spain
[d] IKERBASQUE, Basque Foundation for Science, 48013 Bilbao, Spain

ARTICLE INFO

Keywords:
Sensors
Zinc oxide
Silver
Gauge factor
Dc magnetron sputtering
Electromechanical properties

ABSTRACT

This work reports on the preparation and characterization of zigzag nanostructured silver (Ag) doped zinc oxide (ZnO) films in order to improve piezoresistive response for pressure sensor applications. ZnO/Ag thin films were prepared by Glancing Angle Deposition (GLAD) from a metallic zinc (Zn) target DC sputtered in Ar + O_2 atmosphere. The target was customized with different amounts of Ag pellets, symmetrically distributed along the preferential erosion area.

It is shown that increasing the Ag content from 0 to 36 at.% in the ZnO/Ag system leads to a decrease of the electrical resistivity from 2.95 Ω cm to 1.52 × 10^{-5} Ω cm. The structural characterization of the thin films shows an evolution of the preferential growth, changing from a polycrystalline ZnO hexagonal-like structure, confirmed by the presence of dominant ZnO (002) and ZnO (101) diffraction peaks, to a Ag cubic (fcc)-like structure, as evidenced by the Ag (111), (200) and (220) diffraction peaks. The values of the gauge factor show a strong contribution both from Ag as well as from the zigzag nanostructure to the piezoresistive sensitivity of the films, in particular for Ag concentrations lower than 30 at.%. The tunneling distance between pairs of Ag conductive nanoregions was calculated for the different samples and in three different deformation regions, in order to evaluate its influence on the piezoresistive sensitivity. The results show that a longer distance between Ag particles, which varies from 0.1 to 10 nm, enhances the gauge factor, which ranges from 8 ± 1 to 120 ± 3, respectively.

1. Introduction

Piezoresistive strain sensors react to mechanical deformations by the change of the electrical resistance. Several criteria characterize high-performance strain sensors, including sensitivity (i.e. higher gauge factor, GF), stretchabilty, response time, fabrication cost, and stability. Recently, numerous efforts have been focused on developing flexible, stretchable, and highly sensitive strain sensors due to their wide application areas, including rehabilitation and personal health monitoring [1], wearable electronics devices, such as artificial e-skins [2] or robotic skins [3], among others. For this purpose, several types of flexible and stretchable sensors were proposed through the combination of carbon nanotubes and polymers as the support materials, revealing excellent electrical and mechanical properties [4–6].

By contrast, the relationship between mechanical and electrical behaviors becomes even more important if the proposed systems are prepared in the form of thin films, since their strain sensitivity is expected to be different from those of the bulk materials, due to size effects and the increased relevance of micro and nanostructural features. Some reports proved that the doping an insulating matrix with one or more different metals, including silver (Ag), gold (Au), or copper (Cu), to construct a conductive network [7,8], might be interesting candidates for these kind of applications. Generally, these works were dedicated to evaluate the conductivity and critical metal filler fraction, at which a system exhibits a transition from insulating to conductive behavior, typically explained within the framework of the percolation [9,10]. However, very little works have been focused on the sensing properties of these systems [7,11–13]. Additionally, an emerging and attractive method to fabricate strain sensing materials is being developed [14], aiming at the development of material systems where the

* Corresponding author.
E-mail address: armando.f@fisica.uminho.pt (A. Ferreira).

https://doi.org/10.1016/j.tsf.2019.137587
Received 22 February 2019; Received in revised form 20 September 2019; Accepted 22 September 2019
Available online 12 October 2019

electrode material itself acts as a sensor. This is particularly challenging given the relatively high and complex mechanical solicitations that are expected in several of these applications, i.e. bending, elongation and torsion. Anyway, thin films have been mostly prepared by Physical Vapour Deposition methods, but using the conventional columnar growth (perpendicular to substrate). The piezoresistive response of these conventional columnar thin films shows excessive noise in the electrical response [13,14], which demonstrates its inadequacy for the targeted sensor applications. A valuable alternative to eliminate de excessive noise is the *GLancing Angle Deposition* (GLAD) [15], due to the fact that this technique has the ability to modify the columnar characteristics of thin films [16] in zigzag structures [7] and, indirectly, their physical-chemical responses to strong mechanical solicitations, maintaining the functional properties. Moreover, to improve the mechanical solicitations of the piezoresistive sensors, the most explored solutions use silver as conductive filler, based on indium tin oxide, ITO, [17] and indium zinc oxide, ZnO [18]. However, indium-free ZnO-based compounds are preferable to ITO because of the cost factor, and ZnO is known to be an excellent seed layer for the growth nano particles of Ag and Au in the development of solar cells [19–22].

The present work demonstrates a new approach, based on the optimization of nanostructured zigzag-like ZnO/Ag thin films with different amounts of Ag deposited on flexible polymeric PET - Polyethylene terephthalate substrate by GLAD, for the development of piezoresistive thin film sensors. It is shown that the optimized thin films can be used as flexible and stretchable piezoresistive strain sensors.

2. Experimental details

2.1. Thin film preparation

ZnO/Ag thin films were DC sputtered from a metallic zinc (Zn) target (with dimensions 20 × 10 × 0.6 cm^3 and 99.96 at.% purity), using a custom-made vacuum chamber. The Zn target was customized with different amounts of Ag pellets (with individual area of ~0.2 cm^2), symmetrically distributed along the preferential erosion area (~50 cm^2) [23], Fig. 1a), in order to tune the silver content in the coatings. The Zn target was located at 70 mm from the substrate holder (Fig. 1b).

The incidence angle of the Zn particle flux (α) was determined from the substrate normal, by tilting the substrate holder at 45° [13]. The zigzag-like structures, Fig. 1b), were produced by controlling the orientation of the substrate holder relatively to the impinging sputtered particles. The Zn target was sputtered during 20 min, 4 × 5 min for each chevron component of the zigzag structure, Fig.1b), with a constant argon flow rate of 25 sccm (total pressure of 0.28 Pa). Oxygen was added in the gas atmosphere as the reactive gas, at a flow rate of 16 sccm (corresponding to a partial pressure value of 0.45 Pa). The films were prepared at room temperature conditions, the target currents and potential were kept constant at 40 ± 1 mA and 400 ± 1 V, respectively, with a deposition rate average of 0.83 ± 0.07 nm s^{-1}. A plasma reactor (Zepto) was used to sputter-clean the substrates (glass ISO norm 8037–1 microscope slides, (100) p-type silicon wafers and biaxial oriented PET from *Goodfellow*), using a pure Ar atmosphere at a RF power of 100 W applied for 900 s.

For the different architectures, the β column tilt angle of the columns increases differently with the flux angle α, due to the shadowing effects between columns, among others related with the experimental details.

2.2. Morphological, structural, electrical and electromechanical characterization

The morphology of the ZnO/Ag films were characterized by Scanning Electron Microscopy (SEM), using a NanoSEM - FEI Nova 200 (FEG/SEM) microscope, on fractured cross-section and top view conditions. The composition of pure ZnO and ZnO/Ag thin films was further characterized by EDS (EDAX - Pegasus X4M (EDS/EBSD). The structure of the films was characterized by X-ray diffraction (XRD), using a Bruker D8 discover diffractometer (Cu $\lambda_{K\alpha 1}$ = =1.540600 Å), operating in a θ/2θ configuration. A step of 0.02° per 0.2 s and a 2θ angle ranging from 30 to 72° were selected.

In order to evaluate the piezoresistive properties of the ZnO/Ag films, the samples were tested with a 4-point bending system as described in [7], using a Shimadzu-AG-IS universal testing machine, with a load cell of 500 N. Before that, the electrical resistivity of the ZnO/Ag samples was determined by measuring the electrical current with a Keithley 487 picoammeter/voltage source during the applications of voltages ranging from −10 V to 10 V at a step of 1 V. The piezoelectric sensitivity of the ZnO/Ag samples was quantified by the gauge factor (*GF*), which is defined as the ratio between the variation of the relative electrical resistance and the mechanical deformation applied [24]:

$$GF = \frac{\Delta R/R_0}{\varepsilon} = \frac{\Delta \rho/\rho_0}{\varepsilon} + (1 + 2\upsilon) \quad (1)$$

In Eq. (1), R_0 is the steady-state material electrical resistance (in Ω) before deformation and ΔR is the resistance change (in Ω) caused by the

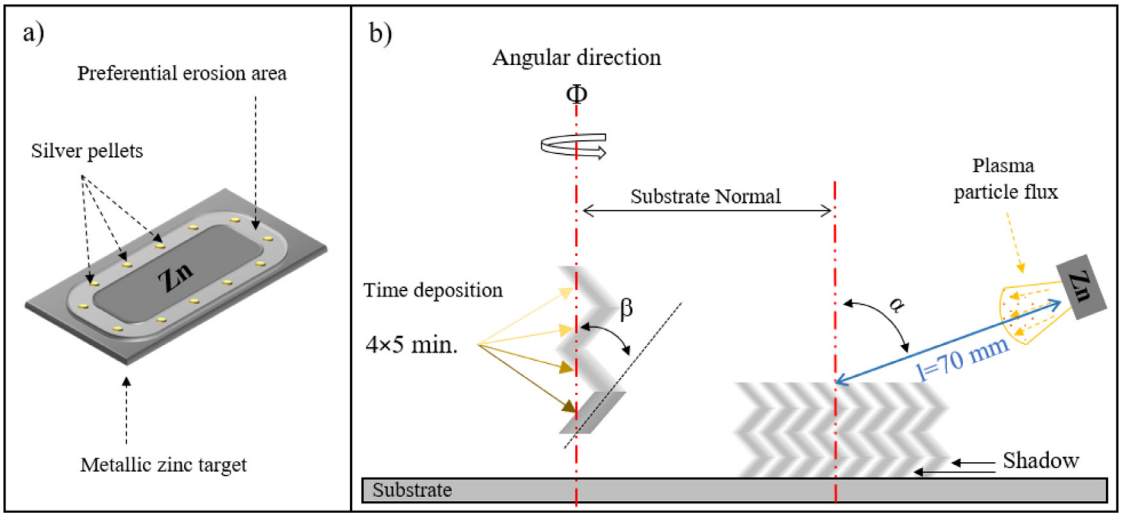

Fig. 1. (a) Schematic representation of the distribution of the Ag pellets on the Zn target and (b) of the GLAD system, where Φ is the angular direction, α is the incidence angle of the Zn particle flux and β is the columnar growth angle.

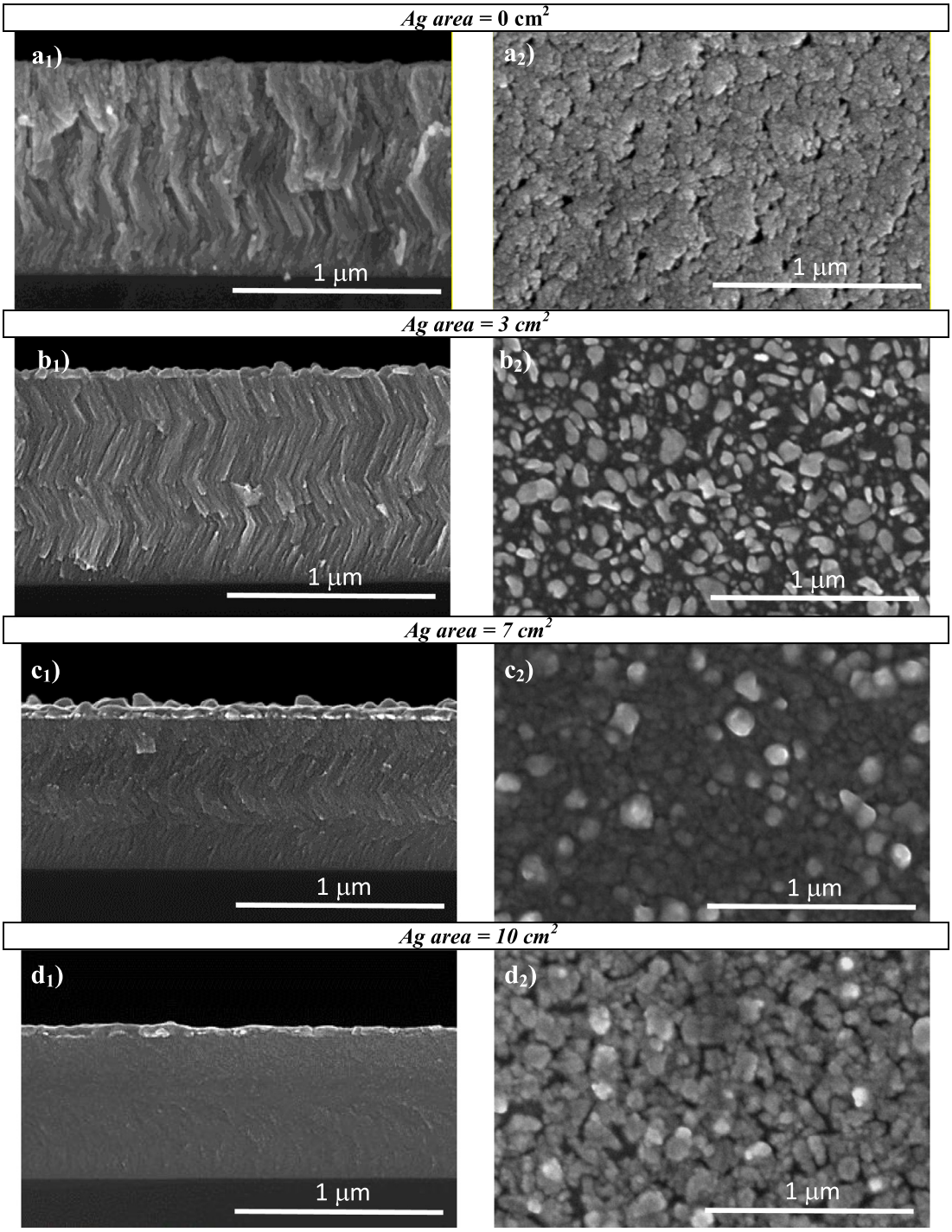

Fig. 2. SEM cross-section and surface views of the ZnO-Ag thin films deposited on silicon prepared using different concentrations of Ag.

mechanical deformation, $\varepsilon = \frac{3dz}{5a^2}$, where d is the thickness of the specimen (film + +substrate), z the displacement applied, a the distance between the first and the second bending points (15 mm). The change of resistance shows contributions from the geometric deformation $(1 + 2\upsilon)$where υs the Poisson ratio and from the relative electrical resistivity change $(\frac{\Delta\rho / \rho_0}{\varepsilon})$Ideally, the Poisson's value assumes the maximum value of 0.5, which means that the geometric effect contribution to the GF is 2 [25].

3. Results and discussion

3.1. Morphological and structural characterization

A set of ZnO/Ag thin films was deposited with increasing Ag contents (obtained by varying the exposed Ag pellets area in the Zn target from 3 to 10 cm^2), with a fixed incident angle $\alpha = =45^\circ$ to obtain zigzag nanostrutures. The representative SEM micrographs of as-deposited samples are presented in Fig. 2.

From Fig. 2, clear changes in the morphologies of the films can be seen with increasing Ag content in the ZnO/Ag thin films. For the sample without Ag, the morphology grows with zigzags structure and

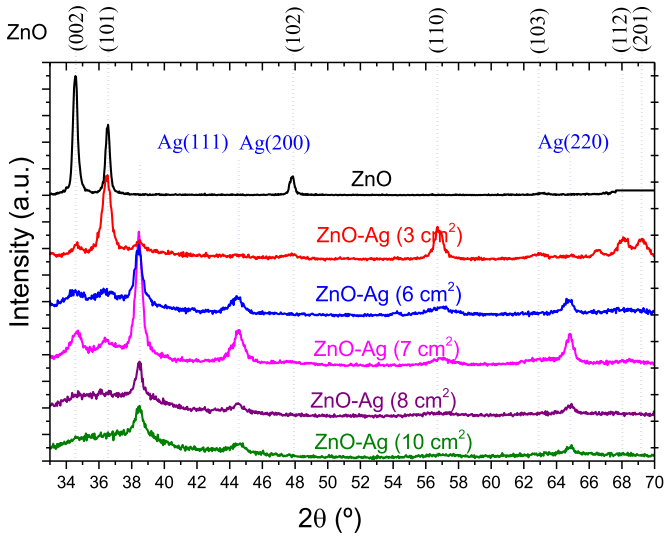

Fig. 3. XRD diffractograms of the nanostructured ZnO/Ag thin films.

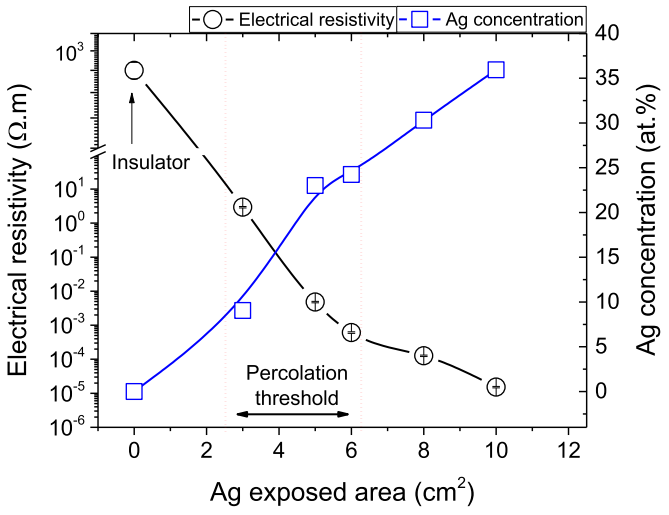

Fig. 4. Room temperature electrical resistivity and Ag atomic concentration as a function of the Ag exposed area.

ended like a "broccoli flower" shape (Fig. 2 a_1 and a_2). Adding Ag to the ZnO films, thin and well-defined zigzags are observed in the ZnO/Ag thin film prepared with an Ag exposed area of 3 cm^2 (Fig. 2 b_1). For the samples with intermediate and highest Ag contents (Fig. 2 c_1 and d_1), the zigzag structure varnishes dramatically, and the films seem to grow denser than the ones prepared with lower Ag contents (Fig. 2 b_1). This tendency can be attributed to the increasing contribution of the Ag exposed area to the "co-deposition" process and the zigzag columns become less defined due to the lower sputtering yield of ZnO [26] when compared to Ag [27]. As a general conclusion, it can be stated that Ag exposed areas below 7 cm^2 seem to be the best experimental conditions in order to obtain clear and well-defined zigzag structures in the ZnO/Ag "co-sputtered" films. Additionally, and as it can be observed in Fig. 2 (b_1 to d_1), increasing Ag contents leads to the formation of a small Ag layer at the top of the surface of the ZnO/Ag thin films, and some relatively large Ag nanoparticles start to appear close to the surface layer. This is expected since some small particles are evenly distributed along the columns due to the high Ag mobility and diffusion ability [28,29].

In order to check if these morphological changes correlated with some changes in the structural features, Fig. 3 shows the XRD patterns of the sputtered ZnO/Ag thin films. It is shown that pure ZnO films develop a polycrystalline hexagonal-like structure, as confirmed by the presence of dominant and very intense ZnO (002) and ZnO (101) diffraction peaks (ICSD database, card #01–070–8070), appearing at angular positions of $2\theta = = 34.4^{\circ}$ and 36.2°, respectively. By increasing Ag content in the films, the ZnO hexagonal (002) preferential growth, which is dominant in the ZnO film, is progressively changed by a (101) one for the films prepared within low exposed Ag area (3 cm^2), as it is observed by the low relative intensity of the diffraction peak located at $2\theta \approx 34.4^{\circ}$ (ZnO (002)). Furthermore, for intermediates exposed areas (6 and 7 cm^2), the hexagonal ZnO (101) growth almost disappears and the fcc-Ag (111) phase (card #04–0783) apprears, as evidenced by the (111) peak, located at $2\theta \approx 38.1^{\circ}$. This growth direction becomes the preferential one. Further, increasing even more the Ag content, the ZnO hexagonal (002) and (101) reveals a mixture of both diffraction growths and the fcc-Ag (111) phase remains the dominant one, which reveals a similar trend as previously observed for the nanostructure variations observed by SEM, Fig. 2.

3.2. Electrical and electromechanical response

The evolution of the electrical resistivity of the ZnO/Ag thin films, as a function of the Ag exposed area on the Zn target surface obtained by EDS, is mainly determined by the Ag concentration (at.%), Fig. 4a). As expected, the electrical resistivity decreases with increasing Ag content in the samples, Fig. 4, which results also in variations of the morphological and structural features, as previously analyzed (Figs. 2 and 3). Several mechanisms have been proposed to explain the electron transport between separate metal islands, including tunnelling [30,31], space-charge limited current flow across the substrate surface, grain boundaries, vacancies, and surface effects [30], among others. Taking into account the existing theories, the results suggest that the decrease of the electrical resistivity is related to the reducing distance between conductive Ag particles, which influences the number of conductive paths and depends on the Ag concentration. The electrical resistivity decreases with the increase of the area of Ag pellets placed on the surface of the Zn target, as shown in Fig. 4. As a general trend, and considering the atomic composition of Ag in the thin films, ZnO/Ag samples exhibit higher resistivity values (2.95 Ω m) for small amounts of Ag pellets. Increasing Ag content leads to a percolation threshold, indicating the transition between states with long- and short-range connectivity between Ag particles. The electrical resistivity decreases further to about 1.52×10^{-5} Ω m for the highest Ag exposed area. It should be noted that this value is still significantly higher than that of bulk silver (1.5×10^{-8} Ω m) which mainly originates, together with the lower Ag concentration, from the polycrystalline film growth with its grain boundaries, defects and surface roughness [32,33].

For sensing applications, the quantification of the electrical variation under bending and the ability of the electrical resistance to return to the initial value after some specific bending cycles are essential parameters. Furthermore, the piezoresistive effect [34], characterized as the sum of two contributions: geometric and structural (Eq.1), is also of paramount importance, giving clear indication of the suitabililiy of a given material to be used in a giving sensor device [35,36]. In order to quantify the piezoresistive response of the ZnO/Ag system, dynamic measurements were performed to determine the films' sensitivity, GF. Fig. 5a) and b) show the variation of the electrical resistance ratio, $\Delta R/R_0$, as a function of time, for a ZnO/Ag thin films with an amount of Ag of 23 at.%, with a z-deformation of 0.5 mm and velocity of 6 mm min^{-1}, during 40 cycles. Fig. 5c) shows the relative resistivity variation, $\Delta R/R_0$, as a function of the applied deformation, ε. Fig. 5d) shows the linear fits of three different regions identified as low, intermediate and high applied deformations, where the GF was mesured, with a speed of 2 mm min^{-1}.

As illustrated in Fig. 5a) and b), the electrical resistance changes with the applied strain, and this tendency is maintained for the different 40 cycles, showing a stable response with no clear aging effect. The sensitivity, GF, for the different samples was obtained from the linear

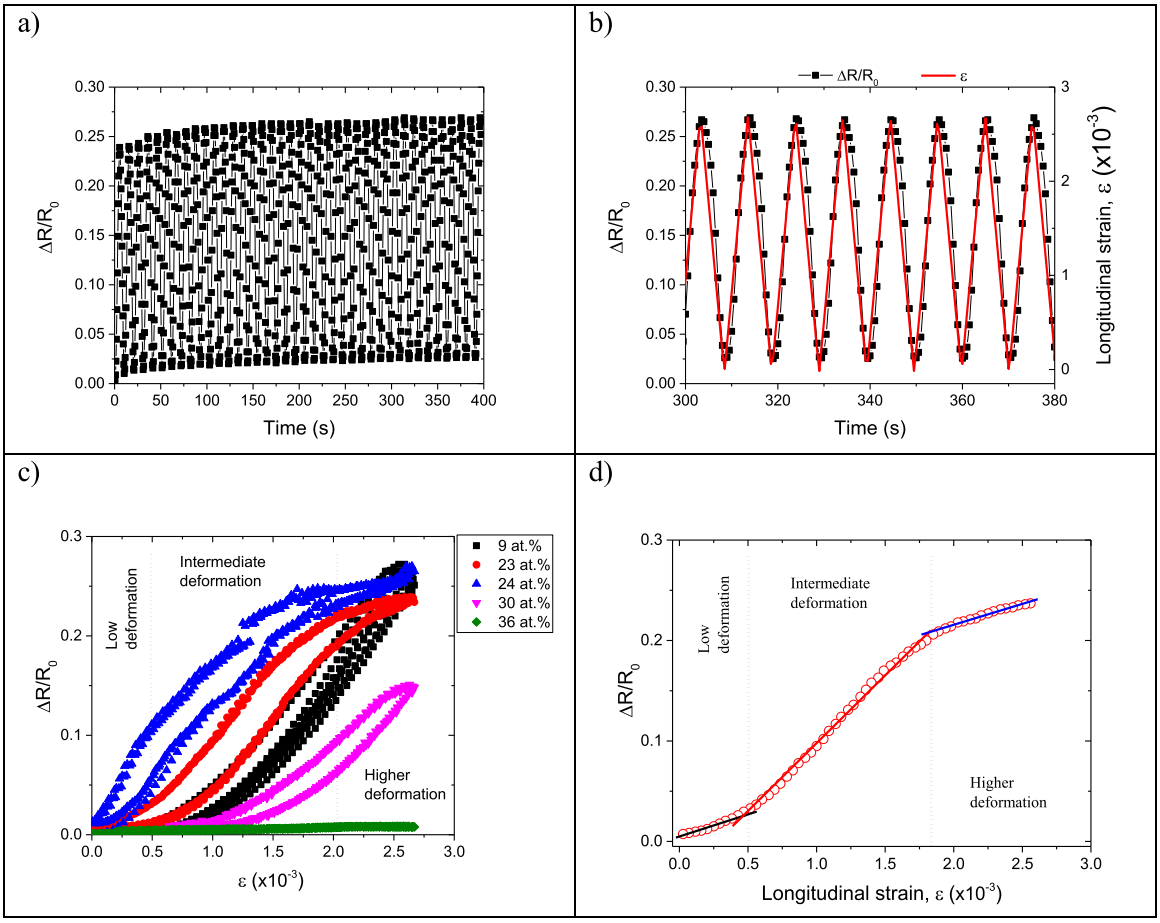

Fig. 5. (a) Electromechanical response after 40 bending cycles for the sample with 23 at.% of Ag with a z-deformation of 0.5 mm and deformation velocity of 6 mm min^{-1}, (b) detail of the electromechanical response of the last 4 cycles, (c) relative resistivity variation, $\Delta R/R_0$, as a function of the applied longitudinal strain, ε. with different amounts of Ag on PET substrates with a deformation velocity of 2 mm min^{-1}, and in (d) is the linear fits of three different regions identified as low, intermediate and high applied deformations to obtain the GF on the loading deformation.

Table 1
Gauge factor values resulting of $\Delta R/R_0$ as function of stress for zigzag structures calculated in the three different regions of deformation.

Ag (at.%)	$GF_{(Low)}$	$GF_{(Intermediate)}$	$GF_{(Higher)}$
9	8 ± 1	120 ± 3	177 ± 1
23	19 ± 1	122 ± 2	67 ± 3
24	78 ± 7	98 ± 4	45 ± 4
30	4 ± 1	64 ± 3	135 ± 2
36	8 ± 1	2.4 ± 0.1	0.8 ± 0.2

fits of three different regions identified in Figs. 5c) and 5d). The slope of the linear fit, obtained from Eq. (1), corresponds to the GF of the sample. The results are presented in Table 1. Each value of GF is the mean value measured in the last 4 cycles of the 40 cycles. The relative resistivity variation, $\Delta R/R_0$, as a function of the longitudinal strain, ε, indicates that the electrical resistivity variation of all samples increases with the applied deformation, but is not linear for the full ε range, because the electromechanical behaviour of the ZnO/Ag thin films was hysteretic (Fig. 5c). In all cases, except for the sample with 36 at.% were the effect does not exist; the electrical resistivity was observed to be higher during the unloading path than during the loading path. This behavior will be discussed later in the text. As a general trend, the values of the gauge factor, Table 1, show a strong intrinsic contribution of the Ag to the sensitivity of the films. In particular, for the samples with 9 at.% and 30 at.% Ag the GF increases in the all regions of deformation. For the sample with 9 at.% Ag, increasing the deformation from low to intermediate values, the gauge factor changes from 8 ± 1 to 120 ± 3, and this trend is maintained with increasing Ag content up to 30 at.%. For an amount of Ag of 36 at.%, the electrical resistivity is relatively low (1.52×10^{-5} Ω m). Consequently, the contribution of the Ag to the GF, for intermediate and higher deformations is only due to the geometric effects, Eq. (1). It is also found that the sample with a Ag content of 24 at.% is the most sensitive to the variation of applied strain. Besides, it is observed that in the region close to 20 at.% of Ag, at which the resistivity decreases heavily, Fig. 4; the largest GF were observed, Table 1. However, due the pronounced hysteretic behavior (Fig. 5c) of the samples in this region, increasing the deformation from intermediate to higher deformations, the GF reduces from 122 ± 2 to 67 ± 3 and from 98 ± 4 to 45 ± 4 for the samples with 23 at.% and 24 at.% respectively. On the other hand, for samples with low and higher amounts of Ag the hysteretic behavior is not so pronounced and disappear for the sample with 36 at.% of Ag. One possible explanation for the unexpected difference in the piezoresistive hysteresis of the samples could be attributed to the geometry of the Ag layer at the top of the surface of the ZnO/Ag thin films (Fig. 2). Moreover, the unchanged initial electrical resistance ($\Delta R/R_0$), after 40 cycles, is particularly relevant to applications as piezoresistive pressure sensors. The initial increase of the resistance observed for the initial cycles, is well related to the strain relaxation of the as-deposited films [7].

Another explanation to the referred resistance variation, $\Delta R/R_0$, could be due the formation of micro-cracks in the films [37]. Fig. 6 shows SEM micrographs taken on the surface of the ZnO/Ag films with 23 at.% Ag, deposited on PET substrates, after 40 cycles bending.

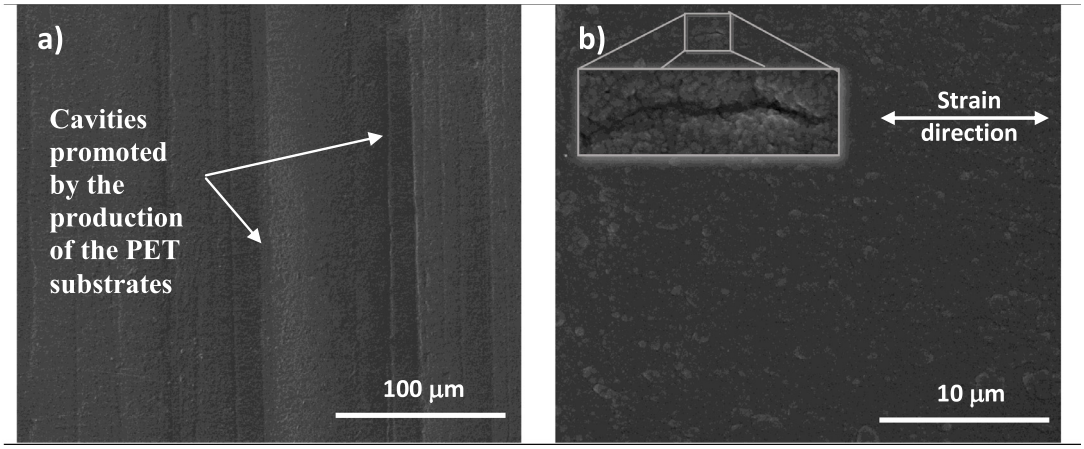

Fig. 6. SEM micrographs of samples with 23 at.% Ag after bending with different magnifications, (a) and (b), measured on polymer substrates (PET).

Fig. 6a) show large cavities and tracks aligned along the surface of the samples, Fig. 6a).

The formation of cavities and tracks is intimately related to the presence of surface depressions or surface roughness, induced by the polymer substrate morphology. According to Dong et al. and Smith et al. [38,39], atoms being deposited in the neighbourhood of a polymer surface cavity will be attracted by the sides of the surface cavity. As a result, the thin film grows aligned with the cavities and with the same orientation of the surface roughness. In our study, the cavities and tracks do not show any clear evidence of fractures along the strain direction (Fig. 6b)). As a result, it is concluded that the film deforms homogenously and the electrical resistivity is not affected by micro-cracks, showing the robustness and reliability of ZnO/Ag thin films for electromechanical applications.

Considering as main explanation the tunneling effect [31], one may suggest that $\Delta R/R_0$ increases/decreases under stretching due to the increased/decreased separation of conductive particles pairs, which influences the distance of conductive paths, So, the three distinct stages, Fig. 5c) and d), are dominated by the variation of the distance of the conductive Ag particles under deformation, leading to variations of the tunneling distance. This mechanism depends on Ag concentration and is associated with an electromechanical hysteresis (Fig. 7). After the first loading-unloading cycle, there is a competitive behavior between the destruction and reformation of conductive networks, Fig. 7a), which tends to level off with increased number of cycles, Fig. 7b).

The repeated piezoresistive behavior of the ZnO/Ag thin films considered here can be entirely explained by the increment/reduction in the conductive particle's pairs distance along the strain direction. This is because $\Delta R/R_0$ increases when ε increases or vice versa. Consequently, within a complete loading and unloading cycle, the current can travel by tunneling effect through pairs of relatively neighbored Ag particles. The tunneling current between the step pairs is proportional to $Xd.\exp(-Xd)$ [36,37,38], where d is the average tunneling distance between adjacent steps, and X is the tunneling barrier height dependent function. According to the tunneling current expression, the resistance changes corresponding to the average tunneling distance d_0 and the strain ε is expressed as:

$$\ln\frac{R}{R_0} = -\ln(1+\varepsilon) + Xd_0\varepsilon \tag{3}$$

and

$$X = \frac{2\pi}{h}\sqrt{2m\varphi} \tag{4}$$

where h is the Planck's constant, m is the mass of the charge carriers, and φ is the tunneling barrier height [40,41].

The experimental results for electrical resistivity, give the percolation thresholds between 23 at.% and 24 at.% of Ag. These values are the critical filler fraction of Ag in the ZnO samples, at which the electrical response of the material suffers significant variations as a function of dopant concentration. The effect of the dopant concentration takes to a band gap modification of ZnO through metal doping [42]. The ZnO thin

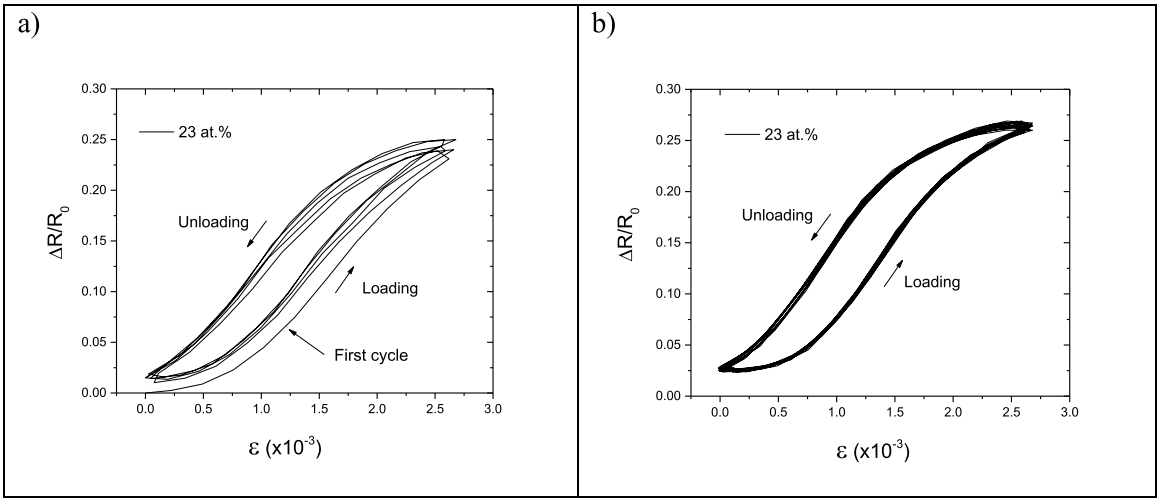

Fig. 7. The relative resistivity variation, $\Delta R/R_0$, as a function of the longitudinal strain, ε, sample with 23 at.%. (a) Electromechanical response for the first 5 bending cycles, (b) for the last 20 bending cycles.

Table 2
Calculated distances between two Ag particles for the different samples using the parameters derived from the fit with Eq. (3) and assuming a barrier height of 3 and 3.4 eV.

Ag (at.%)	$d_{0(Low)}$ (nm)		$d_{0\ (Intermediate)}$ (nm)		$d_{0\ (High)}$ (nm)	
	3 eV	3.4 eV	3 eV	3.4 eV	3 eV	3.4 eV
9	0.5	0.4	6.8	6.4	10.0	9.4
23	1.1	1.0	6.9	6.5	3.8	3.5
24	4.4	4.1	5.5	5.2	2.5	2.4
30	0.2	0.2	3.6	3.4	7.6	7.1
36	0.5	0.4	0.1	0.1	0.5	0.4

film has a direct band gap of Eg ~3.37 eV, with a large exciton binding energy of 60 meV at room temperature. The annealed ZnO/Ag co-sputtered films at the theoretical doping level of 5 at.% and 8 at.% have the corresponding optical energy band gaps between 3.23 and 3.21 eV, respectively [42]. Assuming a band gap values of 3 and 3.4 eV, which include the values for the band gap of the ZnO/Ag thin films, and using Eq. (3) for the tunneling effect through conductive pairs, the values of d_0 as the tunneling distance were calculated and presented in Table 2,

From the change of the Ag interparticle distance, it becomes possible to explain the behavior of the GF in the three different regions. For lower deformations and 3 eV of barrier height, the distance between Ag particles is ~0.5 nm, for the sample with 9 at.%. Increasing stretching leads to increased separation of conductive particles pairs, from 0.5 to 10 nm, reducing the number of conductive paths and consequently increase the $\Delta R/R_0$ leading to higher GF's. These calculations demonstrate that increasing that tunneling distance strongly affects the GF of the ZnO/Ag system. Higher distances between Ag conductive particle pairs imply higher resistivities and consequently higher sensitivity of the transducers. Increasing the barrier height to 3.4 eV for the same sample, the results show a small decrease in the distance between conductive pairs, as actually expected. For lower deformations, the distance reduces to 0.1 nm (from 0.5 to 0.4 nm), while for intermediate deformations, the distance reduces to 0.4 nm (from 6.8 to 6.4 nm). For higher deformations, the reduction is of 0.6 nm, varying from 10.0 to 9.4 nm. However, tunnelling distances of the order of a few nanometres are realistic, although those associated with the higher deformations are relatively larger. Anyway, these are simple estimations of the size of a typical junction. The real system will contain a range of connections with variable parameters. In the present case, the distance is in the range of the numerical results commonly reported in polymers with carbon nanotubes [40,43], where the piezoresistive mechanism and the electrical resistance are dominated by the inter-particle distance variations.

The tunneling resistance variation ratio can be used in this way as a powerful indicator of the strain sensitivity of a ZnO/Ag thin films, controlling both the electrical and electromechanical response of the system.

4. Conclusion

Zigzag-like ZnO/Ag thin films were prepared by GLAD, using a metallic Zn target with different amounts of Ag pellets, symmetrically distributed along the preferential erosion area.

Morphological characterization showed that for small amounts of Ag exposed area (3 cm^2), ZnO/Ag thin film with well-defined zigzag architectures were obtained. For the samples prepared with the highest Ag contents, the zigzag structure becomes less defined, and the films seem to grow denser than the ones prepared with lower Ag contents.

From the structural features, the ZnO/Ag thin film developed a polycrystalline hexagonal-like structure, confirmed by the presence of dominant and very intense h-ZnO (002) and ZnO (101) diffraction peaks. By increasing the Ag content in the films, and for intermediates exposed areas (6 and 7 cm^2), the hexagonal ZnO (101) growth almost vanishes and the fcc-Ag (111) phase apprears. This growth direction became the preferential one, which reveals a similar trend observed for the nanostructure variations observed by SEM.

The change in the electrical resistivity of the ZnO/Ag thin films, due the increasing amount of Ag, induces strong variation of the response of the transducers due to their varying electrical response, which contribute to the variation of the response of the piezoresistive ZnO/Ag system. The results show that the structure has a pronounced influence on the overall transducer response. Increasing the deformation from low to intermediate deformations, the gauge factors, increase from 8 ± 1, to 120 ± 3 for 9 at.% Ag. This trend is maintained with the increment of Ag content until 30 at.% Ag. After 40 bending cycles, the ZnO/Ag thin films do not show any clear evidence of fractures along the strain direction, which illustrates this ZnO/Ag thin film is very robust and reliable for sensing applications.

Acknowledgements

This work was supported by the Portuguese Foundation for Science and Technology (FCT) in the framework of the Strategic Funding UID/FIS/04650/2013 and project PTDC/EEI-SII/5582/2014. Armando Ferreira acknowledges the FCT for the SFRH/BPD/102402/2014 grant. Funding was also provided by the Region of Franche-Comté, the French RENATECH network. This work has also been supported by the EIPHI Graduate School (contract "ANR-17-EURE-0002"). Financial support from the Basque Government Industry Department under the ELKARTEK and HAZITEK programs is also acknowledged.

References

[1] A. Ferreira, V. Correia, E. Mendes, C. Lopes, F. Vaz, S. Lanceros-Mendez, Piezoresistive polymer-based materials for real-time assessment of the stump/socket interface pressure in lower limb amputees, IEEE Sens. J 17 (2017) 2182–2190, https://doi.org/10.1109/JSEN.2017.2667717.
[2] X. Shuai, P. Zhu, W. Zeng, Y. Hu, X. Liang, Y. Zhang, R. Sun, C.P. Wong, Highly sensitive flexible pressure sensor based on silver nanowires-embedded polydimethylsiloxane electrode with microarray structure, ACS Appl. Mater. Interfaces 9 (2017) 26314–26324, https://doi.org/10.1021/acsami.7b05753.
[3] N. Lu, D.-H. Kim, Flexible and stretchable electronics paving the way for soft robotics, Soft Robot 1 (2014) 53–62, https://doi.org/10.1089/soro.2013.0005.
[4] A. Ferreira, S. Lanceros-Mendez, Piezoresistive response of spray-printed carbon nanotube/poly(vinylidene fluoride) composites, Compos. Part B Eng. 96 (2016) 242–247, https://doi.org/10.1016/j.compositesb.2016.03.098.
[5] L. Arboleda, A. Ares, M.J. Abad, A. Ferreira, P. Costa, S. Lanceros-Mendez, Piezoresistive response of carbon nanotubes-polyamides composites processed by extrusion, J. Polym. Res. 20 (2013) 326–337, https://doi.org/10.1007/s10965-013-0326-y.
[6] P. Costa, A. Ferreira, V. Sencadas, J.C. Viana, S. Lanceros-Méndez, Electro-mechanical properties of triblock copolymer styrene-butadiene- styrene/carbon nanotube composites for large deformation sensor applications, Sensors Actuators A 201 (2013) 458–467, https://doi.org/10.1016/j.sna.2013.08.007.
[7] A. Ferreira, J. Borges, C. Lopes, N. Martin, S. Lanceros-Mendez, F. Vaz, Piezoresistive response of nano-architectured TixCuy thin films for sensor applications, Sensors Actuators A 247 (2016) 105–114, https://doi.org/10.1016/j.sna.2016.05.033.
[8] F. Guo, X. Zhu, K. Forberich, J. Krantz, T. Stubhan, M. Salinas, M. Halik, S. Spallek, B. Butz, E. Spiecker, T. Ameri, N. Li, P. Kubis, D.M. Guldi, G.J. Matt, C.J. Brabec, ITO-free and fully solution-processed semitransparent organic solar cells with high fill factors, Adv. Energy Mater 3 (2013) 1062–1067, https://doi.org/10.1002/aenm.201300100.
[9] P. Sheng, B. Abeles, Y. Arie, Hopping conductivity in granular metals, Phys. Rev. Lett. 31 (1973) 44–47, https://doi.org/10.1103/PhysRevLett.31.44.
[10] P. Smilauer, Thin metal films and percolation theory, Contemp. Phys. 32 (1991) 89–102, https://doi.org/10.1080/00107519108213805.
[11] P. Pedrosa, A. Ferreira, N. Martin, M. Arab Pour Yazdi, A. Billard, S. Lanceros-Méndez, F. Vaz, Nano-sculptured Janus-like TiAg thin films obliquely deposited by GLAD co-sputtering for temperature sensing, Nanotechnology 29 (2018) 355706–355717, https://doi.org/10.1088/1361-6528/aacba8.
[12] A. Ferreira, N. Martin, S. Lanceros-Méndez, F. Vaz, Tuning electrical resistivity anisotropy of ZnO thin films for resistive sensor applications, Thin Solid Films 654 (2018) 93–99, https://doi.org/10.1016/j.tsf.2018.03.090.
[13] A. Ferreira, J. Borges, C. Lopes, M.S. Rodrigues, S. Lanceros-Mendez, F. Vaz, Relationship between nano-architectured Ti1 − xCux thin film and electrical resistivity for resistance temperature detectors, J. Mater. Sci. 52 (2017) 4878–4885, https://doi.org/10.1007/s10853-016-0722-x.
[14] A. Ferreira, C. Lopes, N. Martin, S. Lanceros-Méndez, F. Vaz, Nanostructured

functional Ti-Ag electrodes for large deformation sensor applications, Sensors Actuators 220 (2014) 204–212, https://doi.org/10.1016/j.sna.2014.09.031.
[15] T.G. Knorr, R.W. Hoffman, Dependence of geometric magnetic anisotropy in thin iron films, Phys. Rev 113 (1959) 1039–1046, https://doi.org/10.1103/PhysRev.113.1039.
[16] P. Pedrosa, A. Ferreira, J.M. Cote, N. Martin, M.A.P. Yazdi, A. Billard, S. Lanceros-Mendez, F. Vaz, Influence of the sputtering pressure on the morphological features and electrical resistivity anisotropy of nanostructured titanium films, Appl. Surf. Sci 420 (2017) 681–690, https://doi.org/10.1016/j.apsusc.2017.05.175.
[17] M. Fahland, P. Karlsson, C. Charton, Low resisitivity transparent electrodes for displays on polymer substrates, Thin Solid Films 392 (2001) 334–337, https://doi.org/10.1016/S0040-6090(01)01053-7.
[18] S.H. Cho, W.J. Lee, Effect of added metallic elements in ag alloys on the durability against heat and humidity of indium zinc oxide/Ag alloy/indium zinc oxide transparent conductive multilayer system, Jpn. J. Appl. Phys 49 (2010) 111102, , https://doi.org/10.1143/JJAP.49.111102.
[19] M. Arbab, Base layer effect on the d.c. conductivity and structure of direct current magnetron sputtered thin films of silver, Thin Solid Films 381 (2001) 15–21, https://doi.org/10.1016/S0040-6090(00)01341-9.
[20] J. Luo, Y.X. Wang, J. Sun, Z.S. Yang, Q.F. Zhang, MnS passivation layer for highly efficient ZnO–based quantum dot-sensitized solar cells, Sol. Energy Mater. Sol. Cells 187 (2018) 199–206, https://doi.org/10.1016/J.SOLMAT.2018.07.012.
[21] X. Wang, Y. He, M. Chen, Y. Hu, ZnO-Au composite hierarchical particles dispersed oil-based nanofluids for direct absorption solar collectors, Sol. Energy Mater. Sol. Cells 179 (2018) 185–193, https://doi.org/10.1016/J.SOLMAT.2017.11.012.
[22] W. Zhao, H. Li, Z. Liu, D. Wang, S. (Frank) Liu, Controlled defects and enhanced electronic extraction in fluorine-incorporated zinc oxide for high-performance planar perovskite solar cells, Sol. Energy Mater. Sol. Cells 182 (2018) 263–271, https://doi.org/10.1016/J.SOLMAT.2018.03.047.
[23] R.P. Domingues, M.S. Rodrigues, M. Proença, D. Costa, E. Alves, N.P. Barradas, F.J. Oliveira, R.F. Silva, J. Borges, F. Vaz, Thin films composed of Au nanoparticles embedded in AlN: influence of metal concentration and thermal annealing on the LSPR band, Vacuum 157 (2018) 414–421, https://doi.org/10.1016/j.vacuum.2018.09.013.
[24] S. Beeby, G. Ensell, M. Kraft, N. Whit, e, MEMS Mechanical Sensors, Artech House, Boston, 2004, https://doi.org/10.1017/CBO9781107415324.004.
[25] M. Bao, Analysis and Design Principles of MEMS Devices, Elsevier Science, 2005, https://doi.org/10.1016/B978-0-444-51616-9.X5000-0.
[26] C.R. Aita, A.J. Purdes, K.L. Lad, P.D. Funkenbusch, The effect of O2on reactively sputtered zinc oxide, J. Appl. Phys. 51 (1980) 5533–5536, https://doi.org/10.1063/1.327472.
[27] N. Maréchal, E. Quesnel, Y. Pauleau, Silver thin films deposited by magnetron sputtering, Thin Solid Films 241 (1994) 34–38, https://doi.org/10.1016/0040-6090(94)90391-3.
[28] P. Pedrosa, E. Alves, N.P. Barradas, N. Martin, P. Fiedler, J. Haueisen, F. Vaz, C. Fonseca, Electrochemical behaviour of nanocomposite Agx:tin thin films for dry biopotential electrodes, Electrochim. Acta 125 (2014) 48–57, https://doi.org/10.1016/j.electacta.2014.01.082.
[29] J. Kulczyk-Malecka, P.J. Kelly, G. West, G.C.B. Clarke, J.A. Ridealgh, K.P. Almtoft, A.L. Greer, Z.H. Barber, Investigation of silver diffusion in TiO2/Ag/TiO2coatings, Acta Mater. 66 (2014) 396–404, https://doi.org/10.1016/j.actamat.2013.11.030.
[30] G. Dittmer, Electrical conduction and electron emission of discontinuous thin films, Thin Solid Films 9 (1972) 317–328, https://doi.org/10.1016/0040-6090(72)90122-8.
[31] L. LeBlanc, Under-balanced drilling solution for wells with long reservoir exposure, Offshore 55 (1995) 37–51, https://doi.org/10.1038/srep11939.
[32] K. Fuchs, The conductivity of thin metallic films according to the electron theory of metals, Math. Proc. Cambridge Philos. Soc 34 (1938) 100–108, https://doi.org/10.1017/S0305004100019952.
[33] A.F. Mayadas, M. Shatzkes, Electrical-resistivity model for polycrystalline films: the case of arbitrary reflection at external surfaces, Phys. Rev. B 1 (1970) 1382–1389, https://doi.org/10.1103/PhysRevB.1.1382.
[34] L.E. Hollander, G.L. Vick, T.J. Diesel, The piezoresistive effect and its applications, Rev. Sci. Instrum 31 (1960) 323–327, https://doi.org/10.1063/1.1716967.
[35] J. Lintymer, J. Gavoille, N. Martin, J. Takadoum, Glancing angle deposition to modify microstructure and properties of sputter deposited chromium thin films, Surf. Coatings Technol 174–175 (2003) 316–323, https://doi.org/10.1016/S0257-8972(03)00413-4.
[36] G.Y. Huang, C.Y. Wang, J.T. Wang, First-principles study of diffusion of Li, Na, K and Ag in Zno, J. Phys. Condens. Matter. 21 (2009) 345802, , https://doi.org/10.1088/0953-8984/21/34/345802.
[37] O. Glushko, V.M. Marx, C. Kirchlechner, I. Zizak, M.J. Cordill, Recovery of electrical resistance in copper films on polyethylene terephthalate subjected to a tensile strain, Thin Solid Films 552 (2014) 141–145, https://doi.org/10.1016/j.tsf.2013.12.055.
[38] L. Dong, R.W. Smith, D.J. Srolovitz, A two-dimensional molecular dynamics simulation of thin film growth by oblique deposition, J. Appl. Phys. 80 (1996) 5682–5690, https://doi.org/10.1063/1.363621.
[39] R.W. Smith, D.J. Srolovitz, Void formation during film growth: a molecular dynamics simulation study, J. Appl. Phys. 79 (1996) 1448–1457, https://doi.org/10.1063/1.360983.
[40] A. Ferreira, M.T. Martínez, A. Ansón-Casaos, L.E. Gómez-Pineda, F. Vaz, S. Lanceros-Mendez, Relationship between electromechanical response and percolation threshold in carbon nanotube/poly(vinylidene fluoride) composites, Carbon N.Y. 61 (2013) 568–576, https://doi.org/10.1016/j.carbon.2013.05.038.
[41] J. Zhao, C. He, R. Yang, Z. Shi, M. Cheng, W. Yang, G. Xie, D. Wang, D. Shi, G. Zhang, Ultra-sensitive strain sensors based on piezoresistive nanographene films, Appl. Phys. Lett 101 (2012) 063112, , https://doi.org/10.1063/1.4742331.
[42] F.C. Liu, J.Y. Li, T.H. Chen, C.H. Chang, C.T. Lee, W.H. Hsiao, D.S. Liu, Effect of silver dopants on the ZnO thin films prepared by a radio frequency magnetron co-sputtering system, Mater. (Basel) 10 (2017) 797, https://doi.org/10.3390/ma10070797.
[43] R. Rahman, P. Servati, Effects of inter-tube distance and alignment on tunnelling resistance and strain sensitivity of nanotube/polymer composite films, Nanotechnology 23 (2012) 055703, , https://doi.org/10.1088/0957-4484/23/5/055703.